

Characterization And Numerical Optimization Of Chromium Free Nickel Alloy Filler-Materials For Dissimilar Welding With SS304 Based On Induced Residual Stresses And Distortion

Vivek Vanamane*, Santhosh kumar B**, Nataraj J. R.***

Department of Mechanical Engineering, R. V. College Of Engineering, Bangalore-59

Abstract

The aim of the work was to study and optimize among eight different Cr free Ni based filler materials of chemical composition of wt% ranging between 40-43.5Ni, 4-20Mo, 0-16Co, 10Cu, 22-25Fe, 0.5Al, 1Ti, 0.001C. The alloys developed were characterized for their metallurgical phases and mechanical properties in both as-cast and solution treatment (at 1100 °C) conditions using JMatPro V6 (materials simulation software). The dissimilar welding of SS 304 with these alloys is simulated using the birth and death technique in ANSYS. Numerical Optimization was performed based on the induced stresses present in the weld joint which are one of the main factors to cause failures in dissimilar weld joints. For welding simulation, the eight noded SOLID 70 elements were used for thermal stress analysis and SOLID 45 elements were used for structural analysis. The FEM simulation results show the longitudinal residual stresses along the weld line, tensile stresses developed around 80 MPa occur at the middle of the weld. The maximum vertical deflection of 0.325 mm was observed for the alloy of composition 43.499Ni, 0.5Al, 14Co, 6Mo, 10Cu, 23Fe, 2Mn, 1Ti, 0.001C. On the other hand the minimum vertical deflection of 0.2 mm and residual stress of 50MPa was observed in alloy of composition 39.999Ni, 0.5Al, 20Mo, 10Cu, 22Fe, 6.5Mn, 1Ti, 0.001C.

Keywords: Alloy development, birth and death technique, Finite Element Method, residual stress, Welding Simulation.

1. Introduction

New chromium free Nickel based welding filler materials for welding stainless steel were simulated using JMatPro V6-materials simulation software). During TIG welding of stainless steel, carcinogenic Hexavalent Chromium Cr⁺⁶ fumes are generated from the weld pool which can cause the welders respiratory problems including lung cancer. OSHA in its new guidelines has reduced the Permission Exposure limit to 5µ/mm³ as explained in the Welding Journals by Susan R. Fiore[1-2]. In 2008, J. M. Vitek [3] demonstrated about how computational thermodynamics could be used to

identify the compositional requirements to avoid the formation of deleterious phases such as eta phase, sigma phase and P-phase. Numerical simulation of welding process using Finite Element Method (FEM) has been proved to be a powerful and useful method to predict the welding temperature field, residual stress field and deformation owing to the fact that, measurement of residual stress by experimental techniques has certain practical limitations. Experimental techniques may be destructive as the hole-drilling technique or even when non-destructive techniques are used (e.g. X-ray diffraction technique), residual stress can be measured only at discrete locations near the weld surface. The cost of performing these experiments would be a concerning factor, especially if large number of measurements are to be done. Lindgren [4] gave a detailed account of the application of the Finite Element Method to predict the thermal, material and mechanical effects of fusion welding from the 1970s to 2003. Chang and Teng et al [5] performed thermal elasto-plastic analyses using the finite element techniques to obtain the residual stresses in the butt-welded joints. Goldak [6] introduced a 3D model for heat source generation. Though, 3D heat source modeling provided accurate results but it requires lots of computation time.

In the recent years, numerical optimization of various welding filler materials has been performed. H. Naffakh [7] has performed dissimilar welding of AISI 310 austenitic stainless steel to nickel-based alloy Inconel 657, but no one has yet performed the numerical optimization of chromium free nickel alloy filler materials based on the induced residual stress in welding. This investigation performs thermal elasto-plastic analysis using finite element techniques to evaluate the residual stresses in dissimilar welding. In this work about eight version of chromium free Ni alloy filler materials of chemical composition varying from 40-43.5%Ni, 4-20%Mo, 0-16%Co, 10%Cu, 22-25%Fe, 0.5%Al, 1%Ti, 0.001%C are optimised by determining the induced residual stresses using numerical simulation. A 2D surface heat flow model was implemented and the longitudinal and transverse stress distribution was determined for all the alloys. Based on the results of the analysis, the most suitable alloy for production of filler material for stainless steel welding is determined.

2. Alloy Composition

Table 1 shows the chemical composition of the various Nickel alloy filler materials considered for simulations. Cobalt, Iron, Molybdenum, Titanium, and Aluminum are all solid-solution hardeners in Nickel. Cobalt having good solubility of other alloying elements was varied from 0-16 wt%. Cobalt wt% was balanced with Molybdenum wt%. Cobalt provides the dispersion of strengthening intermetallic particles. Higher Cobalt content imparts better wear resistance but less desirable polishability and machinability [1]. The beneficial influence of C in reducing sigma phase is due to the fact that higher C leads to more carbide formation. The production of Ni based alloy for welding electrodes has been increasing each year owing to its good weldability, resistance to ductile dip cracking [8], hot cracking susceptibility, less carbon diffusion and high strength [9].

3. JMatPro Results

The various compositions were given in JMatPro software to determine the phases present at varying temperatures. The phases present at 600°C are given in fig 1.

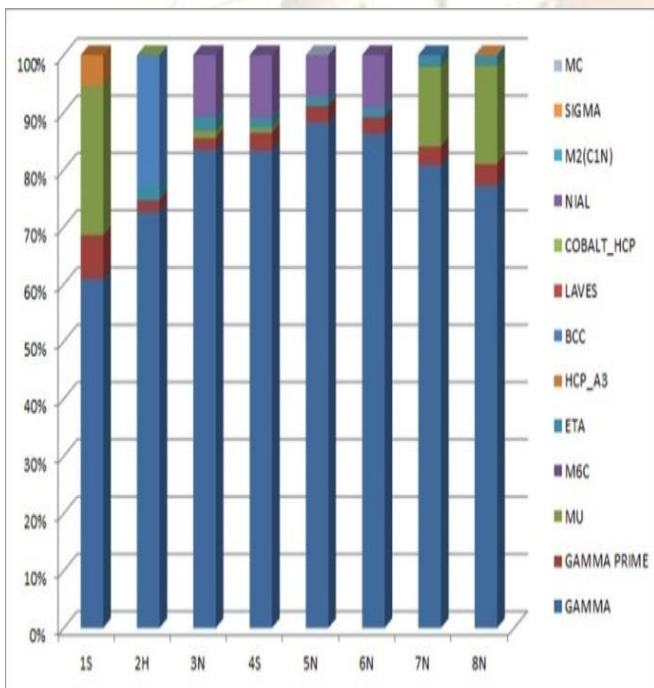


fig 1: % of phases of different alloys at 600°C

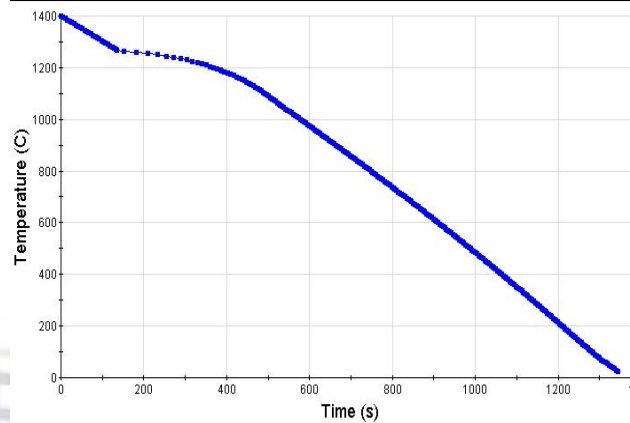


fig 2: JMatPro predicted Cooling Curve for Alloy 1S

Ni-20.0Mo-10.0Cu-22.0Fe-6.5Mn-1.0Ti-0.5Al-0.001C wt(%)

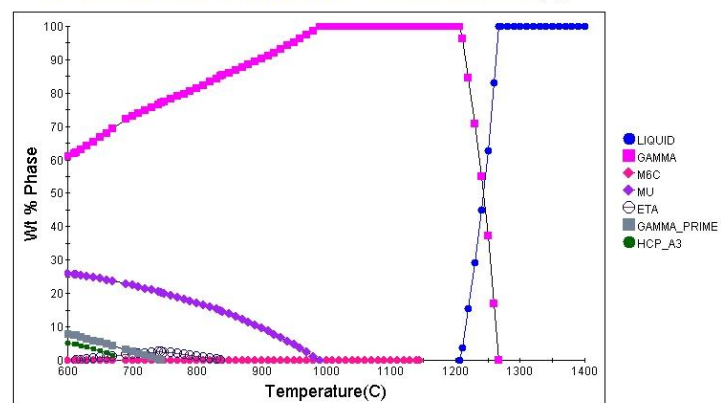


fig 3: JMatPro predicted phase diagram of alloy type-1S

4. Experimental Results

The cooling curves and microstructure of Alloy 1S was obtained experimentally and compared with JMatPro results. fig 2 predicts the cooling curve for the alloy type 1S, solidification begins at temperature 1270°C and ends at 1200 °C. JMatPro predicts existence of only liquid phase at the temperature above 1270°C as shown in fig 3. γ -solid solution phase exists between 1270-1200°C. Formation of MC type carbides phase is predicted at 1150°C. As the temperature falls below 990°C potentially undesirable phases including μ (μ) and eta η (eta) phase is predicted to form. γ' (Gamma prime) precipitate phase is predicted to solidify below 750°C. In fig 4 DSC spectrum confirms the prediction of JMAT Pro and fig 5 confirms the presence of alloying element in the XRD analysis.

Table: 1 Chemical composition of different version of Ni based alloys.

Alloy	Ni %	Fe %	Mo %	Co %	Cu %	Mn %	Ti %	Al %	C %
1S	39.999	22	20	Nil	10	6.5	1	0.5	0.001
2H	43.499	25	20	Nil	10	Nil	1	0.5	0.001
3N	43.499	25	10	10	10	0	1	0.5	0.001
4S	43.499	23	10	10	10	2	1	0.5	0.001
5N	43.499	23	6	14	10	2	1	0.5	0.001
6N	43.499	23	8	12	10	2	1	0.5	0.001
7S	43.499	23	12	8	10	2	1	0.5	0.001
8N	43.499	23	14	6	10	2	1	0.5	0.001

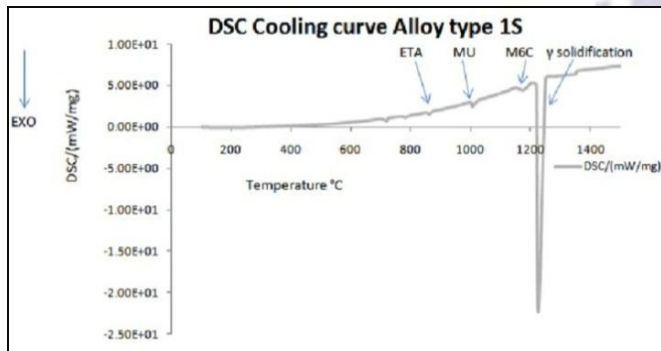


fig 4: DSC cooling curve of Alloy type 1S

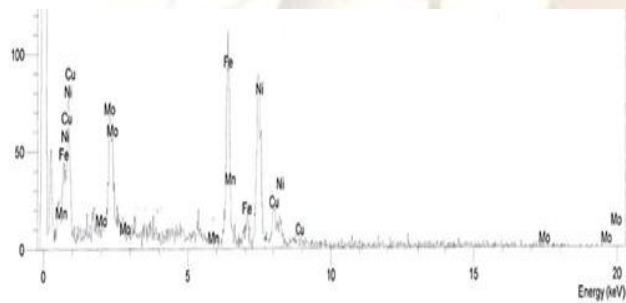
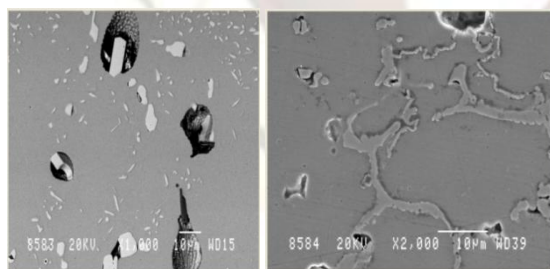


fig 5: The XRD analysis of the 1S alloy confirms the presence of Ni, Mo, Mn, Cu, Fe alloying elements.



a) As cast b) Solution Treated
 fig 6: SEM Microstructures of Alloy

Patches of lamellae, are clearly resolved at higher magnifications. In fig 6 Light, globular particles are M_6C ; gray particles are MC carbide. Structures consist of nickel-rich γ solid-solution matrix containing a few light-etching carbide particles and dispersed γ' . JMatPro also indicates the presence of M_6C phase and MC carbide as shown in fig 1 for 1S alloy.

5. Thermo-Mechanical Analysis

In this section, a sequential thermo-elastic plastic three-dimensional finite element computational procedure is developed to calculate temperature field, residual stresses and distortions. The procedure begins with a nonlinear transient thermal analysis and the temperature histories are applied as thermal loads in a nonlinear transient structural analysis to obtain the residual stresses and distortions.

6. Specimen and Material Properties

fig. 7 shows two plate sections that are joined by a single-pass butt-weld. The length, width and thickness of the plate are assumed to be 140, 300 and 5 mm, respectively [10].

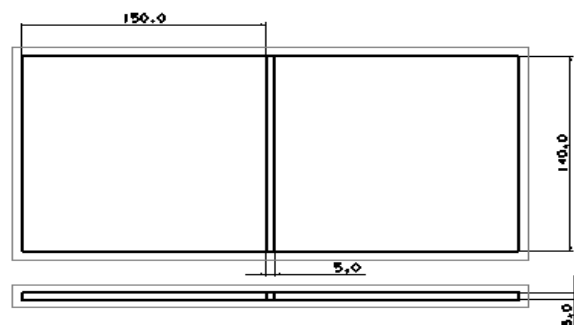


fig. 7 Shows two plate sections that are joined by a single-pass butt-weld

Both thermal and mechanical material properties of 304 Stainless Steel were considered to be temperature-dependent and are given in Table 2. The thermal and mechanical properties of the 8 alloys were obtained using JMAT Pro (Materials simulation software) and are given in the figures 8-11.

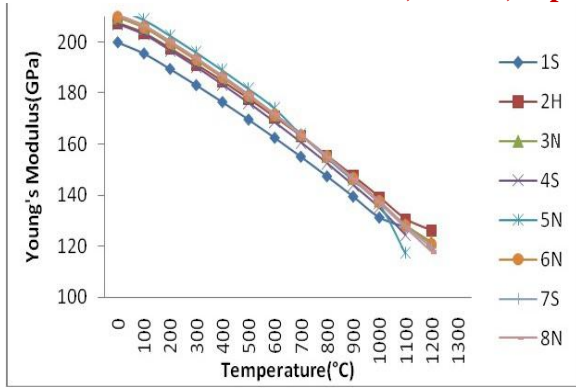


fig 8: Variation of Young's Modulus of all alloys with Temperature.

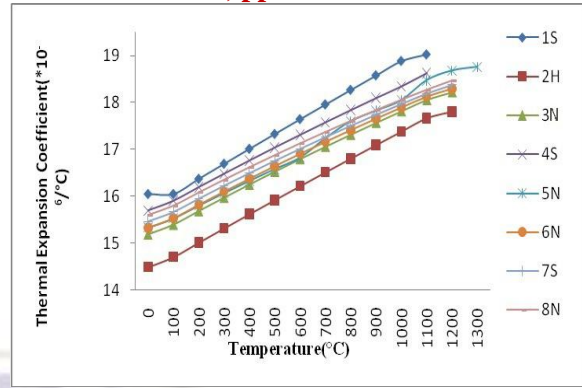


fig 10: Variation of Thermal Expansion Coefficient of all alloys with Temperature.

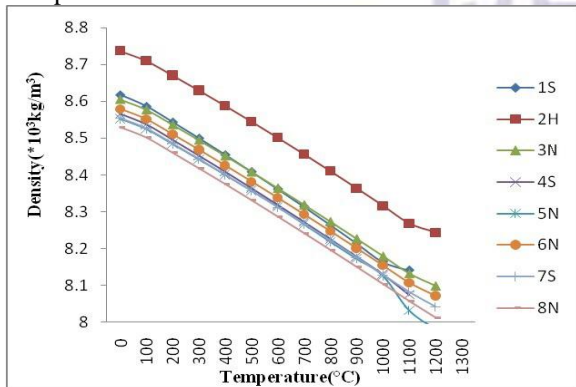


fig 9: Variation of Density of all alloys with Temperature.

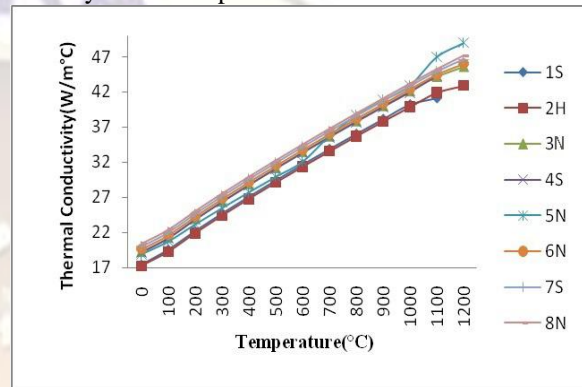


fig 11: Variation of Thermal Conductivity of all alloys with Temperature.

Table 2. Thermal and mechanical material properties of SS304.

Temperature (°C)	Thermal expansion Coefficient (*10 ⁻⁶ /°C)	Thermal conductivity (W/m°C)	Density (kg/m ³)	Specific heat (J/kg)	Young's Modulus (GPa)
25	14.3489	16.76606	7749.77	462	206.21187
100	14.3489	17.68191	7724.83	481.6	201.92657
200	14.69002	18.90059	7690.46	517.8	195.4473
300	15.03217	20.11912	7654.84	558.4	187.84373
400	15.37537	21.34275	7618	608.6	179.11943
500	15.71961	22.56949	7579.98	676.6	169.38741
600	16.0649	23.78245	7540.8	784.4	158.8054
700	16.41122	24.97985	7500.51	714.6	147.55249
800	16.75859	26.17949	7459.14	672.4	135.82023
900	17.10699	27.38602	7416.72	665.6	123.80936
1000	17.45644	28.59459	7373.29	671.6	111.72867
1100	17.80693	29.80303	7328.89	683.8	99.7936
1230	18.26413	31.37344	7269.79	746.6	84.8664
1350	18.29934	31.55186	7269.79	859.03	84.8669

7. 3D FE Model

The three-dimensional finite element model used in this simulation is shown in fig 12. The model has 1148 elements and 2438 nodes after meshing.

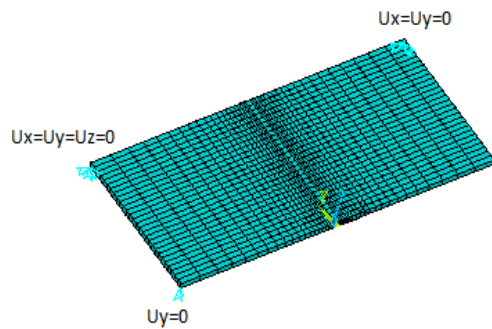


fig 12: The finite element mesh for the single-pass butt-weld.

The finite element meshes used for both thermal and structural analyses are the same, except for the element type. For thermal analysis, solid 70, an eight-node, first order brick element with temperature degree of freedom at each node is used. For structural analysis, solid 45, an eight-node, first order brick element with three translational degrees of freedom. The constraints are provided as shown in fig 6 in order to allow free distortion of the plate during welding [11].

8. Thermal Analysis

The transient temperature during welding is determined by the three-dimensional nonlinear heat transfer equation:

$$\rho C \frac{\partial T}{\partial t} = \frac{\partial}{\partial X} \left(k \frac{\partial T}{\partial X} \right) + \frac{\partial}{\partial Y} \left(k \frac{\partial T}{\partial Y} \right) + \frac{\partial}{\partial Z} \left(k \frac{\partial T}{\partial Z} \right) + Q, \quad (1)$$

Where ρ is density, C is specific heat, k is thermal conductivity, Q is the rate of internal heat generation, T is temperature, t is time, and X, Y and Z are coordinates in the reference system. Convection heat transfer with a heat transfer coefficient of $15 \text{ W/m}^2\text{C}$ is applied to all free surfaces [12]. Radiation heat transfer is ignored. Table 3 shows the welding parameters chosen for this analysis.

Table 3: Shows the welding parameters chosen for this analysis [13]

Sl No	Parameter	Value
1	Welding Method	TIG
2	Current (I)	110 A
3	Voltage (V)	20 V
4	Welding Speed (v)	5 mm/s

The heat sources are applied along the weld path for practical welds. A Gaussian power distribution with an arc radius of 2.82 mm was assumed for the heat flux. The power distribution

was defined relative to a coordinate system that was moving with the heat source is expressed as:

$$Q' = \left(\frac{r}{c} \right) = \frac{3Q}{\pi c^2} e^{-3r^2/c^2} e^{-3y^2/c^2} \quad (2)$$

Where c is the arc radius, the total net heat input was calculated as:

$$Q = \eta UI \quad (3)$$

Where η is the arc efficiency which is considered as 85%.

This study simulates weld thermal cycle for SS 304 steel as shown in fig 13.

The heating cycle takes 28 load steps increment with a time step of 1s and the modified Newton Raphson method was used in each time step for the heat balance iteration. Max temperature of 1300°C is achieved during welding.

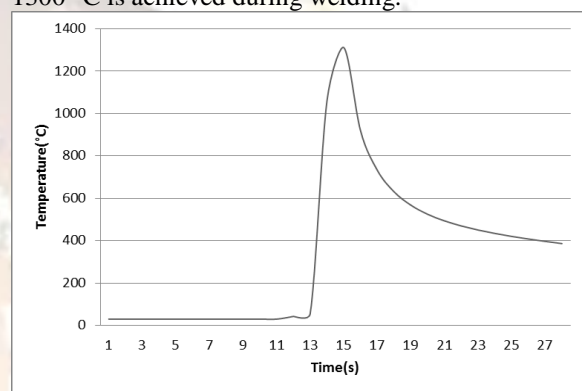


fig 13: Simulated weld Thermal cycle for SS304 steel

9. Results and discussion

9.1 Longitudinal residual stresses

Longitudinal stresses are the stresses acting parallel to the weld bead and are denoted by σ_y . fig. 14 illustrates the distributions of the residual stress σ_y along the X-direction (at $Y = 70 \text{ mm}$) for all the 8 alloys. High tensile stresses arise in regions near the weld due to a resistance contraction of the material as cooling commences [12]. The stress distribution is compressive in nature in the base metal region. The minimum tensile residual stress of 51MPa is obtained for 1S alloy and a maximum tensile stress of 80MPa is obtained for 3N alloy.

9.2 Transverse residual stresses

Transverse residual stresses are the stresses acting perpendicular to the weld bead and are denoted by σ_x . fig. 15 represents the distributions of the residual stress σ_x along the Y-direction for all the alloys. As seen in the figure, the stress distributions are tensile in the middle of the weld and compressive at the ends [12]. The minimum tensile residual stress of 50MPa is obtained for 1S alloy and a maximum tensile stress of 83MPa is obtained for 5N alloy.

9.3 Vertical Deflection

fig 16 shows the vertical deflection (in z direction) along the length of the plates. As this figure reveal, the maximum deflection is around 0.325mm which is sufficiently less. Due to property mismatch, a sharp variation in the deflection at the weld is seen. Alloy 1S has a minimum deflection of 0.25mm at the weld.

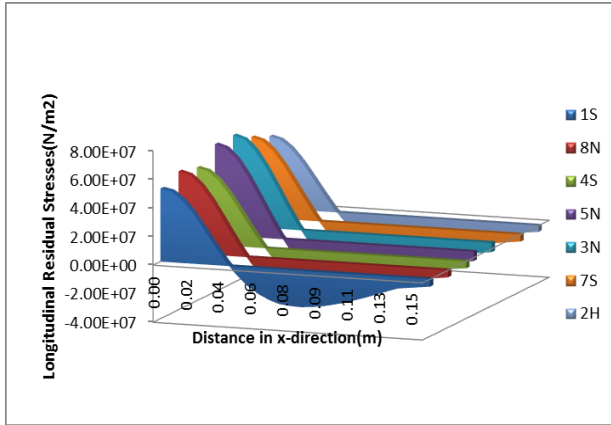


fig 14: Longitudinal residual stress distribution along the X-direction.

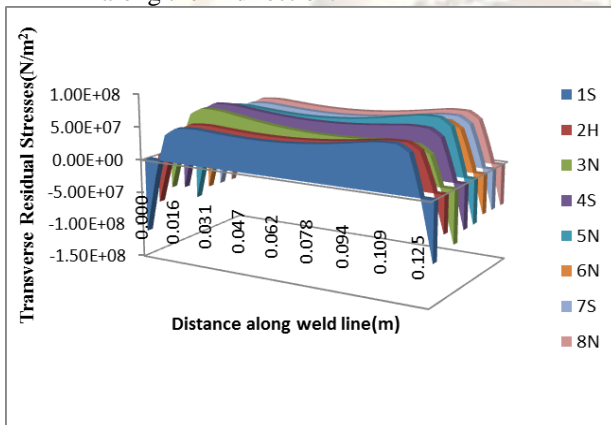


fig 15: Transverse residual stress distribution along the Y-direction.

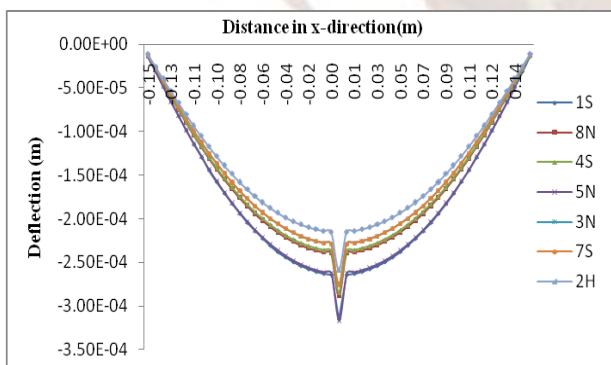


fig 16: Vertical Deflection along the width of the plate.

10. Conclusion

The above study involves the development and optimization of 8 Cr free Ni based filler materials for dissimilar welding of SS304. In the

recent years, the development of Cr free filler materials have been on the rise due to noxiousness of Cr⁺⁶ fumes generated during welding. 8 Ni based alloys with varying composition of Cu, Co, Mn were developed and characterized for their metallurgical phases and mechanical properties in both as-cast and solution treatment (at 1100 °C) conditions using JMatPro V6. The use of JMatPro greatly reduces the cost and time required for the simulation and calculation. This can calculate wide range of materials properties for alloys and is particularly aimed at multi-components alloys used in industrial practice. Numerical Simulation using Finite Element Method reduces the time and cost of performing experimental analysis, especially if large number of measurements are to be done.

The important results and conclusions extracted from this study are listed below.

- The experimental cooling curve of 1S alloy shows the solidification temperature as 1270°C, JMatPro predicts existence of only liquid phase at temperature above 1270°C.
- The phases present at various temperatures as obtained from DSC spectrum matches with the prediction of JMatPro for 1S alloy.
- Numerical simulation of dissimilar welding of SS304 and the 8 alloys were performed using birth and death technique in ANSYS. The variation of residual stresses and distortion were determined.
- A minimum longitudinal tensile residual stress of 51MPa was obtained for 1S alloy and a maximum tensile stress of 80MPa was obtained for 3N alloy.
- The minimum transverse tensile residual stress of 50MPa was obtained for 1S alloy and a maximum tensile stress of 83MPa was obtained for 5N alloy.
- Alloy 1S has a minimum deflection of 0.25mm at the weld.

From the results of Welding Simulation, 1S alloy was found to give less residual stresses and distortion than other alloys. Hence it can be concluded that 1S alloy with composition 39.999Ni, 0.5Al, 20Mo, 10Cu, 22Fe, 6.5Mn, 1Ti, 0.001C is more suitable compared to other alloys for dissimilar welding with SS304. Experimental Investigations can be performed on the weld samples in order to determine the strength and other properties of the weld in the future.

References

- [1] ASM HandBook - Vol 02 - Properties and Selection Nonferrous Alloys and Special-Purpose Materials(ASM International,1990)
- [2] Susan r. Fiore, "Reducing Exposure to Hexavalent Chromium in Welding Fumes"

- Welding Journal, Edison Welding Institute, Columbus, Ohi, August 2006.
- [3] J. M. Vitek, D. W. Gandy2, “alloy development of nickel-based superalloy weld filler metals using Computational Thermodynamics”, 1 Oak Ridge National Laboratory, North Carolina 28262.
- [4] L.-E. Lindgren, Numerical modelling of welding, Computer Methods in Applied Mechanics and Engineering 195 (48–49) (2006) 6710–6736.
- [5] Chang, P.H., Teng, T.L., 2004. Numerical and experimental investigations on the residual stresses of the butt-welded joints. *Comp. Mater. Sci.* 29, 511–522.
- [6] Goldak K, Chakaravarti A, Bibby M. A new finite element model for welding heat sources. *Metallurgical Transactions* 1984;15B:299–305.
- [7] H. Naffakha, M. Shamaniana, F. Ashrafizadeha, Dissimilar welding of AISI 310 austenitic stainless steel to nickel-based alloy Inconel 657, *Journal of Materials Processing Technology* Volume 209, Issue 7, 1 April 2009, Pages 3628–3639.
- [8] Gasem M Fallatah, Anwar K Sheik, Zafarullah khan, John K Boah, “Reliability of dissimilar metal welds subjected to sulfide stress cracking”, *The 6th Saudi Engineering conference*, KFUPM, Dhahran, vol.5, De-2002, 297-312.
- [9] Changheui Jang, Jounghoon Lee, Jong Sung Kim, Tae Eun Jin, “Mechanical property variation within Inconel 82/182 dissimilar metal weld between low alloy steel and 316 stainless steel” *International Journal of Pressure Vessels and Piping* 85 (2008) 635–646.
- [10] M. Seyyedian Choobi, M. Haghpanahi and M. Sedighi. “Investigation of the Effect of Clamping on Residual Stresses and Distortions in Butt-Welded Plates”, *IIW International Congress on Welding & Joining*, Tehran, Iran , 17(5), pp. 387-394(2010).
- [11] Liam Gannon , Yi Liu , Neil Pegg , Malcolm Smith, “Effect of welding sequence on residual stress and distortion in flat-bar stiffened plates”, *Marine Structures* 23 (2010) 385–404.
- [12] Tso-Liang Teng, Peng-Hsiang Chang, Wen-Cheng Tseng. “Effect of welding sequences on residual stresses”, *Computers and Structures* 81 (2003) 273–286.
- [13] V. T. Bhanu Kiran, M. Krishna, Praveen M. and Niranjan Pattar. “Numerical Simulation of Multilayer Hard facing on Low Carbon Steel”, *International Journal of Engineering and Technology*, Vol.3, No.1, February 2011, ISSN: 1793-8236.